

Spatial Filtering Applications from Medical Images to 2D Turbulence Using the Fourth-Order and Shock PDEs Methods in Complex Domain

Tamer Nabil^{1,2} and Waleed Abdel Kareem^{1,3}

¹ Mathematics Department, Faculty of Science, King Khalid University, Abha, Saudi Arabia

² Basic Science Department, Faculty of Computers and Informatics, Suez Canal University, Ismailia, Egypt

³ Mathematics Department, Faculty of Science, Suez University, Suez, Egypt

Abstract

The complex fourth-order as well as the complex shock partial differential equations (PDEs) is introduced for noise removal from medical images and 2D turbulent flow. The Lattice Boltzmann method (LBM) with a single relaxation model is used to obtain the velocity field of the turbulent flow. The two filtering methods are applied against the vorticity field of the flow. Comparisons between the results of the two methods for medical images and 2D turbulence are extensively studied. Investigation and identification of the filtering parameters are also considered. It is shown that the proposed filtering methods are effective for noise removal in both applications. Results indicate that the complex fourth-order PDE method extracts the coherent and incoherent parts more clearly compared with the shock method.

Keywords: *Complex fourth-order and shock PDEs filtering methods, medical images, 2D turbulence*

1. Introduction

Filtering can be considered as one of the most important problems in signal and image processing as well as for studies of turbulent flow. The main objective of a filtering method is to extract the original image from the noisy one. In turbulence studies, the filtering method divides each turbulent flow field into two parts: one is the organized coherent part and the second is the randomly distributed incoherent part.

A large number of filtering methods has been used for denoising, such as wavelet-based filtering that employs nonlinear thresholding [1-4], Curvelets [5, 6], total variation [7,8] and non-local mean filtering[9,10].

In recent years, PDEs start to play an important role for data filtering. Most PDEs filtering methods focused on parabolic equations. Osher and Rudian [11] proposed a hyperbolic equation, called shock filter that can serve as a

stable deblurring algorithm approximating deconvolution. Alvarez and Mazorra [12] were the first to couple shock and diffusion for noise elimination and edge enhancement. Gilboa et al. [13] developed shock filter by adding a complex diffusion term to the shock equation. This new term is used to smooth out noise and indicate inflection points simultaneously. The imaginary value which is an approximated smooth second derivative that scaled by the time was used to control the process. They proved that, the results of this algorithm are robust on removing the signal noise. On the other hand, various approaches for filtering noise based on PDEs have been proposed and they are based on second order PDEs and scale space analysis. The methods include anisotropic diffusion equation [14] and a curve evolution equation that is based on geometric heat flow of the level sets of the data [15, 16]. You and Kaveh [17] found that these methods have been unable to achieve a good trade-off between noise removal and features preservation but they tend to cause the processed to look "blocky". They proposed a class of fourth-order PDEs to optimize the trade-off between noise removal and edge preservation.

The time evolution of the PDEs seeks to minimize a cost functional which is an increasing function of the absolute value of the Laplacian of the image intensity function. In a planar image, the Laplacian of the image tends to zero in its neighborhood and hence these PDEs can remove noise and preserve edges by approximating an observed image with a piecewise planar image.

Lysaker et al. [18] introduced a new method for image smoothing based on a fourth-order PDE model. The model is tested on a broad range of the real medical resonance image both in space and time, as well as on non medical synthesized images. This algorithm demonstrates good noise suppression without destruction of important

anatomical or functional details even at poor signal-to-noise ratio.

Rajan et al.[19] extended the second order nonlinear complex diffusion to fourth order complex PDE which produced a much better results.

There are two aims for this paper: one is to compare and study the performance of the complex shock filter and complex fourth-order PDE filter for filtering medical images. The second is to employ the two proposed methods for coherent vortex extraction from 2D homogeneous isotropic turbulence. To our knowledge, many literatures use wavelet theory analysis [20, 21] for filtering turbulent flow. In wavelet filtering, the total flow is divided into two parts, namely the coherent and incoherent parts. In this paper, we introduce the filtering methods using PDEs in spatial domain rather than transformation of the test data into the frequency domain. This spatial filtering may reduce the numerical errors that occur during the Fourier and wavelet transformations and their inverse. This paper is organized as follows. Sec. 2 discusses the proposed filtering methods and their implementations. Sec. 3 is devoted to discuss the applications of the filtering methods to medical images and 2D turbulence. Results and discussion of the obtained results are introduced in sec.4 and finally sec.5 shows the conclusion of the results.

2. Proposed Filtering Methods

Let $Q(\vec{x})$ be a digital image and $Q_0(\vec{x})$ be its observation with random noise $\psi(\vec{x}), \forall x, y \in \Omega$. The noise is superimposed on the pixel intensity value by the formula

$$Q_0(\vec{x}) = Q(\vec{x}) + \psi(\vec{x}) \quad (1)$$

Assume the noise level is approximately known, i.e.

$$\|Q_0(\vec{x}) - Q(\vec{x})\|_{L^2(\Omega)}^2 = \int_{\Omega} (Q_0(\vec{x}) - Q(\vec{x}))^2 d\vec{x} = \sigma^2 \quad (2)$$

Since noise can be recognized as fast oscillating signals over small areas, the important idea for denoising is to filter out high frequency signals while preserving the important features in the images.

2.1 The Complex-Shock Filtering Method

The complex shock filter for 2D data can be written as [13]

$$\frac{\partial Q}{\partial t} = -\frac{2}{\pi} \arctan(A \operatorname{Im}(\frac{Q}{\theta})) \|\nabla Q\| + \lambda Q_{\eta\eta} + \mu Q_{\xi\xi} \quad (3)$$

With the initial condition

$$Q(\vec{x}, 0) = Q_0 \quad , \quad (4)$$

and the boundary condition

$$\frac{\partial Q}{\partial \vec{N}} = 0 \quad \text{on } (\partial\Omega) \quad , \quad (5)$$

where the complex coefficient $\lambda = re^{i\theta}$ depends on the choice of the polar coordinates r and θ , μ is a real scale, A is a parameter that controls the sharpness of the slope near zero, \vec{N} represents the perpendicular direction to the boundary $\partial\Omega$ of the image, $\eta = \eta(\vec{x})$ is the direction of

∇Q and $\eta = \frac{\nabla Q}{\|\nabla Q\|}$, ξ is the normal vector to η and

$Q_{\eta\eta}, Q_{\xi\xi}$ are the second derivative in the direction of η and ξ respectively.

The condition $\frac{\partial Q}{\partial \vec{N}} = 0$ means that we minimize the

boundary influence. The main properties and advantages of the shock filter for noise removal and edge enhancement can be found in [12]. The Numerical implementation of this model is based on the finite difference method. The finite difference method may be used to solve the PDE of the model by applying the iterative approach as follows.

Assuming Δt is the time step, and the space grids size

$$\Delta x = \Delta y = h = 1 \quad \text{then}$$

$$t = n\Delta t, \quad n = 0, 1, 2, \dots \quad (6)$$

$$x = ih, \quad i = 0, 1, 2, \dots, I \quad (7)$$

and

$$y = jh, \quad j = 0, 1, 2, \dots, J \quad (8)$$

where $I \times J$ is the size of the image.

$$Q_{i,j}^{n+1} = Q_{i,j}^n +$$

$$+ \Delta t \left(-\frac{2}{\pi} \arctan(A \operatorname{Im}(\frac{Q_{i,j}^n}{\theta})) \sqrt{\|\tilde{D}_x Q_{i,j}^n\|^2 + \|\tilde{D}_y Q_{i,j}^n\|^2} + \lambda D_{\eta}^2 Q_{i,j}^n + \mu D_{\xi}^2 Q_{i,j}^n \right) \quad (9)$$

Where \tilde{D}_x, \tilde{D}_y are the first order symmetric approximations in x and y respectively. They are defined as,

$$\tilde{D}_x Q_{i,j}^n = \min(|Q_{i+1,j}^n - Q_{i,j}^n|, |Q_{i,j}^n - Q_{i-1,j}^n|) \quad (10)$$

$$\tilde{D}_y Q_{i,j}^n = \min(|Q_{i,j+1}^n - Q_{i,j}^n|, |Q_{i,j}^n - Q_{i,j-1}^n|) \quad (11)$$

and

$$D_{\eta\eta}^2 Q = Q_{\eta\eta} = \frac{Q_{xx}\|Q_x\|^2 + 2Q_{xy}Q_xQ_y + Q_{yy}\|Q_y\|^2}{\|Q_x\|^2 + \|Q_y\|^2 + \varepsilon} \quad (12)$$

where $\varepsilon = 10^{-6}$ is used to avoid division by zero.

$$D_{\xi\xi}^2 Q = Q_{\xi\xi} = \frac{Q_{xx}\|Q_x\|^2 - 2Q_{xy}Q_xQ_y + Q_{yy}\|Q_y\|^2}{\|Q_x\|^2 + \|Q_y\|^2 + \varepsilon} \quad (13)$$

where

$$Q_{xx}^n = Q_{i+1,j}^n - 2Q_{i,j}^n + Q_{i-1,j}^n \quad (14)$$

$$Q_{yy}^n = Q_{i,j+1}^n - 2Q_{i,j}^n + Q_{i,j-1}^n \quad (15)$$

$$Q_{xy}^n = \frac{(Q_{i,j}^n)_x - (Q_{i-1,j}^n)_x}{2} \quad (16)$$

with the symmetric boundary conditions

$$Q_{-1,j}^n = Q_{0,j}^n, \quad Q_{I+1,j}^n = Q_{I,j}^n, \quad j = 0,1,\dots,J \quad (17)$$

$$Q_{i,-1}^n = Q_{i,0}^n, \quad Q_{i,J+1}^n = Q_{i,J}^n, \quad i = 0,1,\dots,I \quad (18)$$

The scheme is convergent if $\Delta t \leq 0.25 \frac{\cos \theta}{r}$, [13]. For

$r=1$ the convergence condition becomes $\Delta t \leq 0.25 \cos \theta$.

Gilboa [13] proved that $\theta = \frac{\pi}{1000}$ gives the best result

according to experimental tests. In order to be more closely to analytic PDEs, a smaller time step may be used (according to convergent condition) at the beginning of the evolution and θ can be set to a very small value. The iterative scheme is ended if the following condition is satisfied

$$\|Q^{n+1} - Q^n\| \leq 10^{-4} \quad (19)$$

2.2 The Complex Fourth-Order PDE Filtering Method

A Fourth-order PDE filtering method can be written as [17]

$$\frac{\partial Q}{\partial t} = -\nabla^2 (c(\|\nabla^2 Q\|)\nabla^2 Q) \quad (20)$$

and the same initial and boundary conditions (4) and (5) are considered. Here the function $c(\cdot)$ is a positive and non-increasing function and it is defined by

$$c(\|\nabla^2 Q\|) = \frac{1}{1 + (\frac{\|\nabla^2 Q\|}{k})^2} \quad (21)$$

where k is a constant (sometimes called the flow constant or the soft threshold). The complex version of the this model is

$$\frac{\partial Q}{\partial t} = -\nabla^2 (\tilde{c}(\text{Im}(Q))\nabla^2 Q) \quad (22)$$

Where

$$\tilde{c}(\text{Im}(Q)) = \frac{e^{i\theta}}{1 + (\frac{\|\text{Im}(Q)\|}{k\theta})^2} \quad (23)$$

θ also represents the phase angle and $\text{Im}(Q)$ is the imaginary part of the data. This partial differential equation can be solved numerically using the finite difference with the same methodology mentioned in Eqns.6-8 and 17-18. The scheme can be written as

$$\nabla^2 Q_{i,j}^n = Q_{i+1,j}^n + Q_{i-1,j}^n + Q_{i,j+1}^n + Q_{i,j-1}^n - 4Q_{i,j}^n \quad (24)$$

The numerical implementation of this method can be summarized and simplified as follows. First consider the function

$$g_{i,j}^n = (\tilde{c}(\text{Im}(Q_{i,j}^n))\nabla^2 Q_{i,j}^n) \quad (25)$$

under the symmetric boundary condition

$$g_{-1,j}^n = g_{0,j}^n, \quad g_{I+1,j}^n = g_{I,j}^n, \quad j = 0,1,\dots,J \quad (26)$$

and

$$g_{i,-1}^n = g_{i,0}^n, \quad g_{i,J+1}^n = g_{i,J}^n, \quad i = 0,1,\dots,I \quad (27)$$

Finally, the numerical scheme can be finalized in the form

$$Q_{i,j}^{n+1} = Q_{i,j}^n - \Delta t \nabla^2 (g_{i,j}^n) \quad (28)$$

3. Applications of the Filtering Methods

The applications of the two filtering methods are applied against 2D medical images as well as 2D homogeneous turbulence. First the methods are applied to 2D medical images and the important statistical parameters are estimated. Then the estimated parameters are examined in 2D turbulent data. In the following section, the parameters estimation will be considered then in the next section the 2D homogeneous turbulence data will be discussed.

3.1 Filtering Parameters estimation

The filtering methods are examined against several medical test images and here three test images are chosen with a size of 128^2 (Fig.1(a), Fig.2(a) and Fig.2(c)). A Gaussian noise with a standard deviation $\sigma = 20$ is

additively considered in the original image (test image 1) as shown in Fig. 1(b). Also, Fig.2(b) and Fig.2(d) show the second and third test noisy images with standard deviations $\sigma = 10$ and $\sigma = 15$, respectively. Fig.3 shows another test data taken from 2D turbulent flow. The contours show the total vorticity of the turbulent flow.

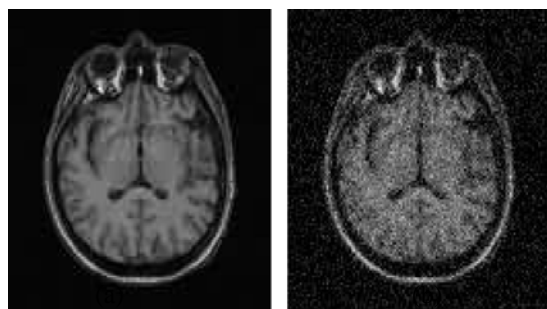
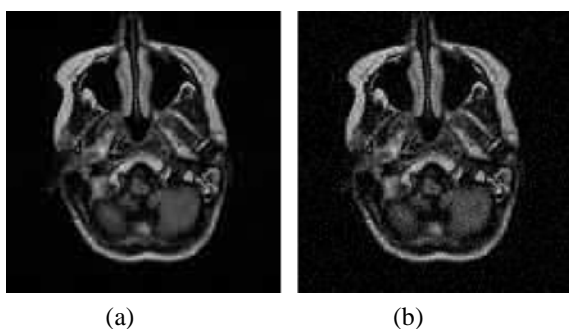
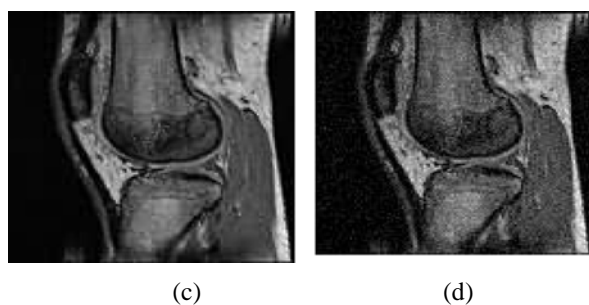


Figure 1: First test image (a) Original image (b) Noisy image



(a)

(b)



(c)

(d)

Fig.2: The second and third test image (a) Original second image (b) Noisy image ($\sigma = 10$) (c) Original third image (d) Noisy image ($\sigma = 15$)

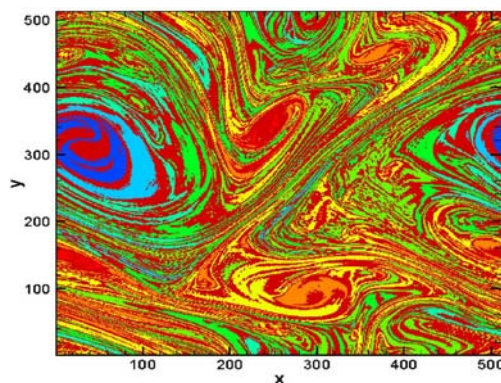


Fig.3: Total vorticity

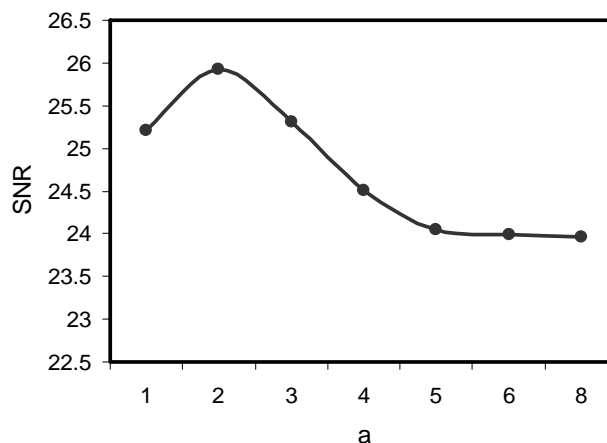


Fig. 4: Complex shock results for the parameter A-estimation

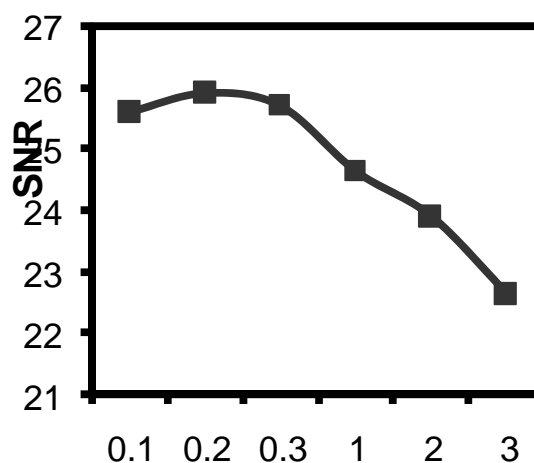


Fig.5: Complex shock results for the parameter μ -estimation

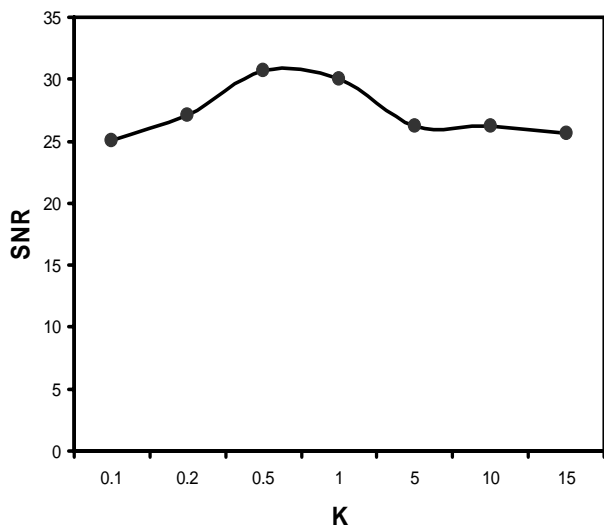


Fig.6: Complex fourth- order results for the parameter K-estimation.

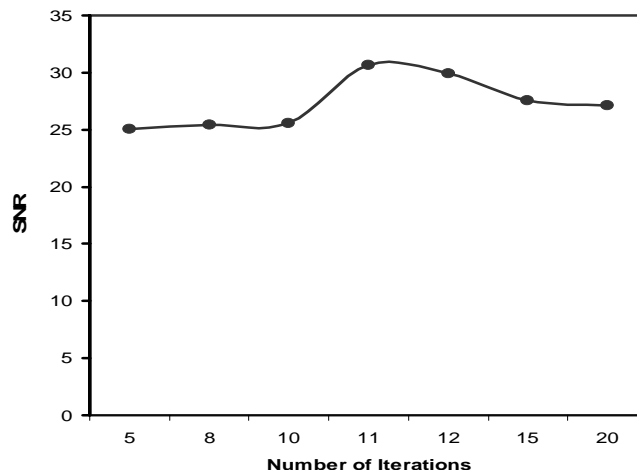


Fig.8: Complex fourth-order results for the number of iterations n convergence

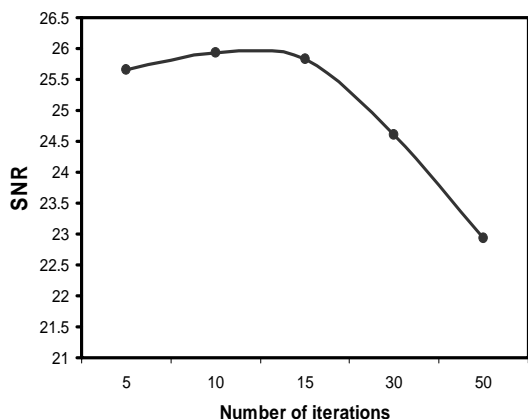


Fig.7: Complex shock results for the number of iterations n-convergence.

Several values of the parameters are tested in the filtering equations to reach the best values of the signal-to-noise-ratio (SNR) which is defined as

$$SNR = 10\log\left(\frac{\sum_{i=1}^N Q_i^2}{\sum_{i=1}^N (\hat{Q}_i - Q_i)^2}\right) \quad (29)$$

where N is the image size. The parameters used in the complex shock method are the phase angle θ , the polar radius r , the constants A and μ . The choices of

$\theta = \frac{\pi}{1000}$ and $r=1$ are based on the study introduced in [13]. The parameters A and μ and the corresponding SNR values are shown in Fig.4 and Fig.5, respectively. It is clear that $A=2$ and $\mu = 0.2$ gives the best SNR values. Also, the soft threshold coefficient k in the complex fourth-order method is chosen as $k=0.5$. Fig.6 shows that at $k=0.5$, the best value of SNR can be reached. The number of iterations n is depicted in Figs. 7 and 8 against the SNR values for the complex shock and complex fourth-order methods, respectively. In the complex shock method the number of iterations $n=10$ leads to the best estimation of SNR as well as it satisfies the convergence condition sated in Eq.19. In the case of the complex fourth-order the value is chosen as $n=11$ for the same reasons. Finally, the time step is chosen as $\Delta t = 0.1$ in the two filtering methods for the stability condition [13].

3.2 2D Homogeneous Turbulence

The lattice Boltzmann method (LBM) is used for simulations of 2D and 3D decaying homogeneous turbulence (e.g. Xu et al.[22] and Abdel Kareem[23]). In this paper the LBM method is used to investigate the 2D

forced turbulence. The velocity data u_x and u_y of a 2D turbulent flow are generated using the $D2Q9$ single relaxation time (SRT) model where, the LBM equation can be written

$$f_\alpha(x + e_\alpha \delta t, t + \delta t) - f_\alpha(x, t) = -\frac{1}{\tau} (f_\alpha(x, t) - f_\alpha^{eq}(x, t)) + 3\rho\omega_\alpha (e_\alpha \bullet F), \quad (30)$$

where $f_\alpha^{eq}(x, t)$ is the equilibrium distribution function. The discrete velocity set and the respective weighting coefficients are e_α and ω_α , respectively. The force

$F = F_x \hat{i} + F_y \hat{j}$ is defined as follows

$$F_x = A \sin(K_y y + \phi) \quad (31)$$

and

$$F_y = A \sin(K_x x + \phi) \quad (32)$$

Here ϕ is the random phase and A is the forcing amplitude.

The equilibrium distribution function is defined as

$$f_\alpha^{eq}(x, t) = \omega_\alpha \rho \left[1 + 3(e_\alpha \bullet u) + \frac{9}{2}(e_\alpha \bullet u)^2 - \frac{3}{2}(u \bullet u) \right], \quad (33)$$

The mathematical definitions of the discrete velocity set and the corresponding weighting coefficients are

$$e_\alpha = \begin{cases} (0, 0, 0), & \alpha = 0 \\ (1, 0), (0, 1), (-1, 0), (0, -1) & \alpha = 1-4 \\ (1, 1), (-1, 1), (-1, -1), (1, -1) & \alpha = 5-8 \end{cases}$$

and

$$\omega_\alpha = \begin{cases} \frac{4}{9}, & \alpha = 0 \\ \frac{1}{9}, & \alpha = 1-4 \\ \frac{1}{36}, & \alpha = 5-8 \end{cases}$$

The simulations are done in a square computation domain with a resolution of 512×512 . The vorticity is calculated from the velocity using the mathematical expression $\nabla \times \vec{u}$ and hence the vorticity can be calculated as

$$\omega = \frac{\partial u_x}{\partial y} - \frac{\partial u_y}{\partial x}. \quad \text{The filtering methods are applied}$$

against the vorticity in the spatial domain. The number of iterations used in the two methods is fixed and it is chosen as $n=10$. This number of iterations leads to a good convergence.

4. Results and Discussion

The shock and fourth-order PDEs filtering methods are applied to different types of data. The first data type is taken from image processing problems and the second type is taken from a study of turbulent flow. The applications of these methods to turbulent flow indicate that moving from image processing filtering to turbulence filtering can be achieved and lead to reasonable and important physical results. These physical results may help understanding important features of turbulence. The important results of the filtering methods can be discussed as follows.

4.1 Complex Shock and Fourth-Order PDEs Filtering Results

Fig.9 shows the denoised and noise image parts using the complex shock method for the first test image. Fig.10 shows the results extracted by the fourth-order method for the first test image, where the denoised and noise image parts are depicted. It can be observed that the extracted denoised image resemble the original image and the noise part doesn't contain any features from the original image. It can be also observed from the results that the method preserves the important features of the original image and isolates the noise from the image in a reasonable way. Figs. 11 and 12 show the filtering results for the second and third test images, respectively. Fig.11(a) shows the denoised image that extracted using the complex shock filtering method. Fig.11(c) shows the denoised image that extracted using the complex fourth-order method. Figs.11(b) and 11(d) show the corresponding extracted noisy parts. Also, Fig.12(a) and (c) show the denoised parts extracted by the complex shock and complex fourth-order, respectively. The removed noisy parts are shown in Figs.12(b) and 12(d), respectively. It is clear that the noisy parts don't include important features from the original images. For turbulent flow, Fig.13 shows the extracted coherent and incoherent parts of the flow field using the complex shock method. It can be observed that the coherent field is similar to the total vorticity field which is depicted in Fig.3. The incoherent part is smoothly distributed along the square region and no coherent regions can be observed.

For the complex fourth-order results that depicted in Fig.14, the coherent and incoherent parts of the flow field are also extracted smoothly. The coherent field is found similar to the total vorticity field and the incoherent part is smoothly distributed along the square region and no coherent regions can be observed.

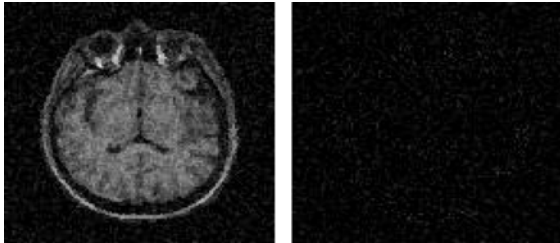


Fig.9: Complex shock results for the test image: (a) denoised (b) noise

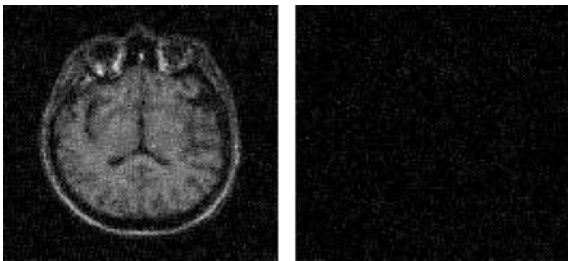


Fig. 10: complex fourth-order results for the test image: (a) denoised (b) noise.

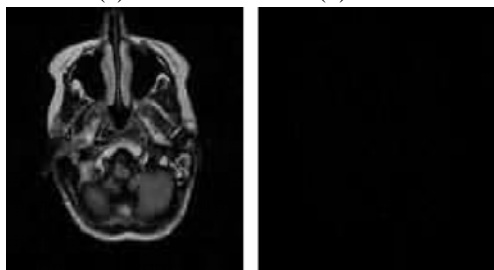
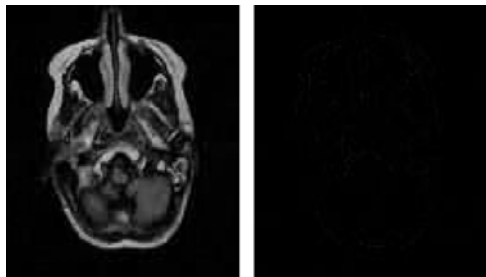


Fig.11: Results for the second test images: (a) denoised by complex shock (b) noise (c) denoised by complex fourth (d) noise

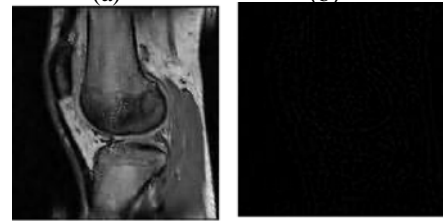
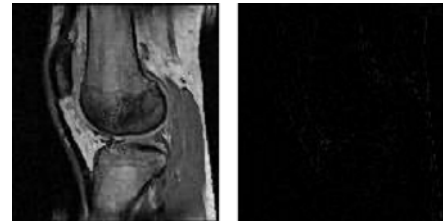


Fig.12: Results for the third test images: (a) denoised by complex shock (b) noise part (c) denoised by complex fourth (d) noise

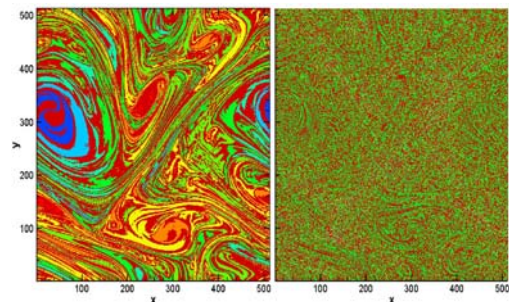


Fig.13: Complex shock results for turbulent flow: (a) coherent part (b) incoherent part

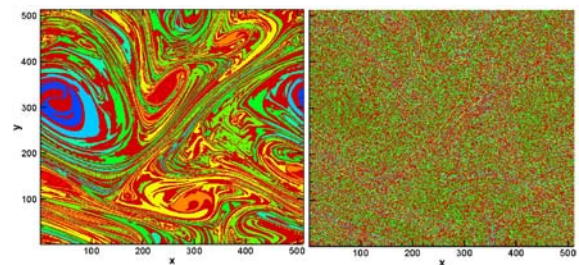


Fig.14: Complex fourth-order results for turbulent flow: (a) coherent part (b) incoherent part

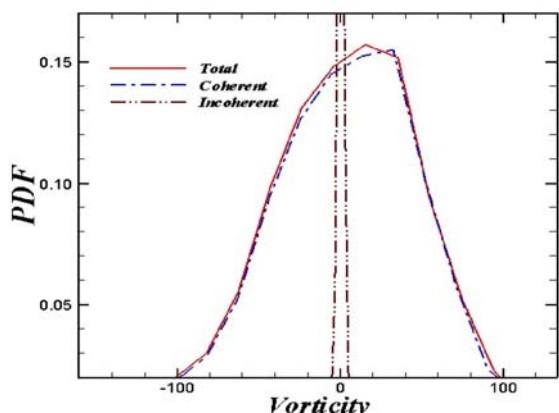


Fig.15: Complex shock: Probability density function (PDF) for the total vorticity, coherent and incoherent parts.

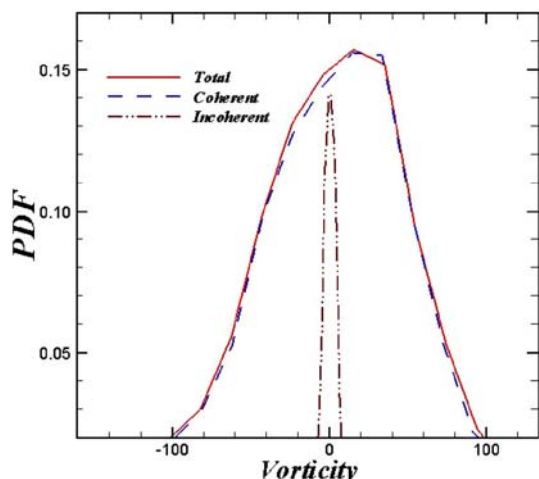


Fig. 16: Complex fourth order: Probability density function (PDF) for the total vorticity, coherent and incoherent parts.

4.2 Analysis and Comparisons of the Filtering Methods

The SNR in the medical image application is found as 25.927 and 30.6712 for the complex shock and complex fourth-order methods, respectively. The noisy image SNR was found as 21.135 which indicate that the two methods are succeeded in the noise removal process. The higher value of the complex-fourth-order SNR indicates that the complex fourth-order is more efficient than the complex shock method. The following tables show the SNR values estimated for the three test images at four different noisy standard deviations.

Table 1: SNR for the first test image

σ	Noisy image	Complex shock	Complex fourth-order PDE
5	35.9874	36.4274	36.9324
10	29.9818	30.8293	31.3778
15	26.2685	28.3086	29.514
20	21.135	25.927	30.6712

The results in the tables support that the fourth-order method is superior to the complex shock filtering method. The SNR values are found larger in all test image cases even at different values of the standard deviation.

Table 2: SNR for the second test image

σ	Noisy image	Complex shock	Complex fourth-order PDE
5	36.231	37.15	39.526
10	33.1873	35.4226	37.3295
15	26.151	27.0219	28.7613
20	23.2150	26.518	29.9814

For the turbulent flow, it can be observed that the complex fourth-order coherent part is more smoothly compared with the complex shock results. It can be observed that some coherent vortices are smoothly visualized using the complex fourth-order results.

Table 3: SNR for the third test image

σ	Noisy image	Complex shock	Complex fourth-order PDE
5	35.0352	36.9761	37.7521
10	32.3156	33.6213	34.8191
15	25.5096	27.0552	29.2892
20	22.5316	28.0532	31.9731

Also, the incoherent part in the complex fourth-order is distributed smoothly in the region. However, some vortical regions, though it is very small, can be observed in the complex shock filtering results. The probability density functions (PDFs) for the total vorticity, coherent and incoherent parts are shown in Figs. 15 and 16. Fig. 15 shows the PDF for the shock results and Fig. 16 shows the results for the fourth-order results. It can be observed that in both cases, the coherent part is almost similar to the total vorticity. The PDF for the incoherent part is Gaussian in both cases. There is a difference between the PDF for the incoherent parts, where in the shock-case a Gaussian PDF with very weak tails can be observed. The PDF for the fourth-order incoherent part is larger than the shock result because in the fourth-order case many noisy regions are extracted without affecting the vortical regions.

5. Conclusions

The complex shock and the complex fourth-order PDEs filtering methods are proposed to extract coherent and incoherent parts of some important experimental data. The test data are of two different types. One of the data set corresponds to medical applications and the second corresponds to turbulent flow. It was shown that the two methods can extract important features in both applications. It was also statistically shown that the complex fourth-order method is superior to the shock method. The characteristics of the extracted coherent and incoherent parts are found similar to previous efforts using the wavelet decompositions. The coherent part is found similar to the non-filtered field and the incoherent part is structuresless. The fourth-order method smoothly extracted the coherent vortices and removed the incoherent background without affecting the geometrical shapes of the vortices.

Acknowledgments

The authors thank the support of King Khalid university (KKU)-Project ID:KKU-SCI-011-008.

References

- [1] D. Donoho and I. Johnston, "Ideal spatial adaptation via wavelet shrinkage", *Biometrika*, Vol. 91, 1994, pp. 425-455.
- [2] D. Donoho, "De-noising by soft thresholding", *IEEE Trans. Inform. Theory*, Vol. 41, 1995, pp. 613-627.
- [3] I.A. Ismail and T.Nabil, "Applying wavelet recursive translation invariant to low-pass filtered images", *Int. J. Wavelets, Multiresolution Inf. Process*, Vol. 2, 2004, pp. 99-110.
- [4] Z. Liu, J. Tian, L. Chen and Y. Wang, "Wavelet-based image denoising variance field diffusion", *Optics Communications*, Vol. 285, 2012, pp. 1744-1747.
- [5] J. Starch, E.Candes and D. Donoho, "The curvelet transform for image denoising", *IEEE Trans. Image Process.*, Vol. 11, 2000, pp. 670-684.
- [6] A.Ali, P.Swami and J. Singha, "Modified curvelet thresholding algorithm for image denoising", *J. Comput. Sci.*, Vol. 6, 2010, pp. 18-22.
- [7] L.Rudin, S.Osher and E. Fatemi, "Nonlinear total variation based noise removal algorithms", *Physica D*, Vol. 60, 1992, pp. 259-288.
- [8] T. Goldsten and S. Osher, "The split Bregman method for L1 regularized Problems", *SIAM J. Imaging Sci.*, Vol. 2, 2009, pp. 323-343.
- [9] A. Buades, B. Coll and J. Morel, "A nonlocal algorithm for image denoising", *Proc. IEEE Int. Conf. On Computer Vision and Pattern Recognition*, Vol. 2, 2005, pp. 60-65.
- [10] M. Mahmoudi and G. Sapiro, "Fast image and video denoising via nonlocal mean of similar neighborhoods", *IEEE Signal Process. Letters*, Vol. 12, 2005, pp. 839-842.
- [11] S. Osher and L. Rudin, "Feature-oriented image enhancement using shock filters", *SIAM J. Num. Anal.*, Vol. 27, 1990, pp. 919-940.
- [12] L. Alvarez and L. Mazorra, "Signal and image restoration using shock filters and anisotropic", *SIAM J. Num. Anal.*, Vol. 31, 1994, pp.590-605.
- [13] G. Gilboa, N. Sochen and Y. Zeevi, "Image enhancement and denoising by complex diffusion process", *IEEE Trans. On Pattern Anal. and Mach. Intell.*, Vol. 25, 2004, pp. 1020-1036.
- [14] P. Perona and J. Malik, "Scale-space and detection using anisotropic diffusion", *IEEE Trans. On Pattern Anal. and Mach. Intell.*, Vol. 12, 1990, pp. 629-639.
- [15] B. Kimia, A. Tannenbaum and S. Zucker, "On the evolution of curve via a function of curvature I", *J. Math. Anal. and Appl.*, Vol. 163, 1992, pp. 438-458.
- [16] G. Sapiro and A. Tannenbaum, "Affine invariant scale-space", *Int. J. Comput. Vis.*, Vol.11, 1993, pp. 25 - 44.
- [17] Y. You and M. Kaveh, "Fourth-order partial differential equations for noise removal", *IEEE Trans. Image Process.*, Vol.9, 2000, pp.1723 - 1730.
- [18] M. Lysaker, A. Lundervold and X. Tai, "Noise removal using fourth-order partial differential equation with applications to medical magnetic resonance image in space and time", *IEEE Trans. Image Process.*, Vol.12, 2003, pp.1579 - 1590.
- [19] J. Rajan, B. Jeurissen and J. Kannan, "Denoising magnetic resonance images using fourth order complex diffusion", *IEEE Int. Mach. Vis. and Image Process. Conf.*, 2009, PP.123 - 127.
- [20] M. Farge, K. Schneider and N. Kevlahan, "Non-gaussianity and coherent simulation for two-dimensional turbulence using an adaptive orthonormal wavelet basis", *Phys. Fluids*, Vol. 11,1999, pp.2187 - 2201.
- [21] M. Farge and K. Schneider, "Coherent vortex simulation (CVS), a semi-deterministic turbulence model using wavelet", *Flow, Turbulence, and Combustion*, Vol.66, 2001, PP.393 - 426.

- [22] H. Xu, Y. Qian and W. Tao, "Revisiting two-dimensional turbulence by Lattice Boltzmann Method ", Progress in Computational Fluid Dynamics, Vol.9, 2009,pp.133 - 140.
- [23] W. Abdel Kareem, "Tracking of vortical structures in three-dimensional decaying homogeneous turbulence ", Int. J. Modern Physics C, Vol.22, 2011, pp.1373 – 1391.

Tamer Nabil received the B.Sc. degree in Mathematics from Faculty of Science, Helwan University at Cairo, Egypt, in 1997, the M.Sc. degree in pure Mathematics from Helwan university at Cairo, Egypt, in 2000, and Ph.D. degree in Computational Mathematics from Suez Canal University at Ismailia, Egypt, in 2005. Currently, he is an Assistant Professor in Mathematics Department, faculty of Science, King Khalid University, Abha, Saudi Arabia. Also, his permanent work is Assistant Professor at Basic Science Department, Faculty of Computers and Informatics, Suez Canal University, Ismailia, Egypt. His research interests are computational harmonic analysis, Numerical methods in Fluid mechanics, and Mathematical methods in image analysis.

Waleed Abdel Kareem received his B.Sc. (1996) and M.Sc. (2001) in Mathematics from Menoufiya University, Faculty of Science, Department of Mathematics, Egypt. In 2006, he received his PhD from Tohoku University, Graduate School of Engineering, Department of Mechanical Systems and Design, Sendai, Japan. Currently, he is Assistant Professor at King Khalid University, Faculty of Science, Department of Mathematics, Abha, Saudi Arabia. His permanent work is Assistant Professor at Suez University, Faculty of Science, Department of Mathematics, Suez, Egypt. His research interests are Lattice Boltzmann method, Turbulent flow and computational harmonic analysis.